SECONDARY FLOW AND HEAT TRANSFER IN A 180-DEGREE SHARP-TURN DUCT WITH DIFFERENT TURN CONFIGURATIONS

Ten-See Wang
Computational Fluid Dynamics Branch
NASA-Marshall Space Flight Center
Marshall Space Flight Center, AL 35812

Mingking K. Chyu
Department of Mechanical Engineering
Carnegie Mellon University
Pittsburgh, PA 15213

ABSTRACT

The numerical results for secondary flow patterns and heat transfer distribution in a two-pass, square duct with a 180-degree sharp turn are presented to examine the effects of three different turning configurations; i.e., (a) straight-corner turn, (b) rounded-corner turn, and (c) circular turn. The simulation employs a non-staggered grid, pressure-based, finite-difference method and solves for three-dimensional transport equations in curvilinear coordinates. Modeling of turbulence uses an extended version of k–ε model. The computed results reveal that secondary flow in the post-turn region displays combined features of a bend-induced, Dean-type circulation and a form-induced separation behind the partition wall. However, the detailed flow structure as well its effect on the local heat transfer varies significantly with different turn configurations. At the turn, the straight-corner case has the strongest turn-induced heat transfer enhancement, while the circular turn has the weakest. In the post-turn region, heat transfer with circular turn surpasses that of the other two configurations, by almost the same difference in the turning region. Average heat transfer results from the present numerical modeling agree favorably with experimental data.

NOMENCLATURE

C_p	pressure coefficient
C_μ	turbulence modeling constant
C_1, C_2, C_3	turbulence modeling constants for ε-equation
D	square channel width
G	diffusion matrix.
h	heat transfer coefficient
J	Jacobian
k	fluid thermal conductivity
L	total streamwise length of sidewall
Nu	Nusselt number
P_k	turbulent kinetic energy production term
p	pressure
S	source term
T	temperature
t	time
U	contravariant velocity
u, v, w	velocity component s
x, y, z	coordinate axes

Greek Symbols

ε	dissipation rate of turbulent kinetic energy
Φ	viscous dissipation function
ϕ	general dependent variable
κ	turbulent kinetic energy
μ	viscosity
ρ	density
σ	turbulence modeling constant
ξ	transformed curvilinear coordinate

Subscript

A	perimeter-averaged, streamwise-resolved
i	at inlet
i,j,k	tensor indices
l	laminar
o	fully developed straight duct without turn
w	wall
τ	turbulent
ϕ	dependent variable

INTRODUCTION

Forced flow through channels connected by 180-degree bends is frequently encountered in various turbomachinery and heat exchanger devices. One of the most notable features in such systems is the effect of the turn-induced secondary flow on the transport phenomena around the bend. Typically, for flows through a curved duct, the imbalance between the radial pressure gradient and the centrifugal force sets up the so-called Dean-type secondary motion (Dean, 1959). The fluid near the mid-plane of the duct moves radially outward, and then moves inward along the top and bottom walls to merge at the mid-plane near the inner wall. Most of the earlier work pertaining to turning flow is primarily directed to the bend geometry having relatively large radii of curvature compared to the channel hydraulic diameter (Mori & Nakayama, 1967, 1971; Cheng & Akiyama, 1970; Humphrey et al., 1977). In such configurations, flow separation is either absent or at least insignificant. Further, heat transfer from the outer (concave) wall is always higher than that from the inner (convex) wall. Several recent studies (Johnson and Launder, 1985; Baughn et al., 1987, Johnson, 1988) on flow through a 180-degree U-bend are also considered to fall into this category.

As a contrast to the mild-bend duct, the present study focuses on a sharp, 180-degree turn with extremely small radius of curvature. Such a geometry is typical for cooling passages inside a rocket nozzle liner or a gas turbine blade or vane. The channel cross-section for both applications often has a very low aspect ratio (about unity), and the flow is generally turbulent. In the open literature, previous studies concerning transport features with a 180-degree sharp turn are directed mostly to turbine blade cooling. Since the mid-1980's, Metzger and his co-workers (Metzger et al. 1984, 1988; Metzger and Sahm, 1986; Fan and Metzger, 1987) at Arizona State University have published a series of studies on surface streakline patterns, pressure measurements, and "regionally local" heat transfer coefficients for a large family of smooth and rough channels. Recently, Chyu (1991) using an analogous mass transfer system have examined both two-pass and three-pass (two turns) channels with rectangular turns. His mass transfer results agree favorably with the heat transfer results reported by Metzger's group. A general observation from all the studies indicates that the flow near the turning region is subjected to vigorous separation, recirculation and reattachment. This results in a highly non-uniform heat transfer distribution.

Compared to its heat transfer counterpart, studies on flow characteristic around a sharp 180-degree turn are relatively fewer and insufficiently understood. Earlier studies in this regard are largely for laminar flow (Murthy and Chyu, 1987; Jiang et al., 1980, Cheng et al., 1992)

rather than turbulent flow. Thus one of the primary motivations of the present research is to obtain detailed information on the turbulent flowfield and its effects on the local heat transfer. Another issue explored here is to examine the influence of turn configuration on the overall transport phenomena in the passage, which is an area little addressed previously. Figure 1 gives schematics of three different turn configurations of present interest; i.e., (a) rectangular turn, (b) rounded-corner turn, and (c) circular-corner turn. The rectangular turn is the most common case when a 180-degree sharp turn is modeled in laboratory and adopted virtually in all of the previous studies. However, due to manufacturing limits, the corners of an actual internal cooling passage can never be perfectly sharp, and the rounded corner is most likely the shape in reality. To a great extent, a rounded-corner turn can be considered to be a combination of both rectangular turn and circular turn. It is expected that the difference in turn geometry can have significant impacts on the nature of flow and heat transfer. Boyle (1984) earlier has measured the regional heat transfer with three turn geometries similar to the present ones. In his study, only the top and bottom walls are heated while the side walls are insulated.

In the present study, the turbulent flowfield and heat transfer in a two-pass channels with the three different turns aforementioned are numerically simulated using a finite difference method. The flow computation undertaken is to solve the incompressible, three dimensional Navier-Stokes equations with an extended k-ε turbulence model. Temperature and heat transfer are calculated by solving the energy equation subsequent to the attainment of a converged velocity field. Except for the details in turn configuration, the channel geometry is virtually the same as that of a rectangular-turn model employed in an experimental study by Chyu (1991). As shown in Figure 1, the channel has a square cross-section with a length of eight channel-width (D), for each pass. The width of the partition wall that separates the two flow passes is one-half the channel width. At the turn, the gap between the tip of the partition wall and the channel outer wall is kept equal to the channel height. For the case of rounded-corner turn, the radius of curvature for the outer wall and at the tip of partition wall is 0.5D and 0.25D, respectively. It is understandable that variation in these turn geometric parameters may yield different results from that of present study. Also shown in Figure 1 is the coordinate system. The z-axis (not shown), along the channel height, is normal to the plane by the right-hand rule.

GOVERNING EQUATIONS AND COMPUTATIONAL SCHEME

The present numerical simulation uses a non-staggered grid, pressure based transport equation solver with an extended version of two-equation k-ε turbulence model (Chen and Kim, 1987). While the computer code has all-speed capability (Chen, 1989; Wang, 1992) for both

compressible and incompressible flows, the present study only uses the incompressible feature. The basic equations employed to describe the momentum and heat transfer in the computational domain are the three-dimensional, Reynolds-averaged transport equations. A generalized form of these equations written in curvilinear coordinates is given by

$$(1/J)(\partial\rho\varphi/\partial t) = \partial[-\rho U_i\varphi + \mu G_{ij}(\partial\varphi/\partial\xi_j)]/\partial\xi_i + (1/J)\, S_\varphi \qquad (1)$$

where J, U_i and G_{ij} represent the Jacobian of the coordinate transformation, contravariant velocities, and diffusion matrices, respectively. They are written as:

$$J = \partial(\xi_i, \xi_j, \xi_k)/\partial(x, y, z) \qquad (2)$$

$$U_i = (u_j/J)(\partial\xi_i/\partial x_j) \qquad (3)$$

$$G_{ij} = (\partial\xi_i/\partial x_k)(\partial\xi_j/\partial x_k)/J \qquad (4)$$

The symbol φ represents a general dependent variable that can be 1, u, v, w, T, k or ε, respectively for the equation of continuity, momentum, energy, turbulent kinetic energy, and turbulent kinetic energy dissipation rate. The symbol ξ is the transformed curvilinear coordinate. $\mu = (\mu_l + \mu_\tau)/\sigma_\varphi$ represents the effective viscosity based on the turbulent eddy viscosity model, where μ_l is the laminar viscosity and $\mu_\tau = \rho C_\mu k^2/\varepsilon$ is the turbulence eddy viscosity. C_μ and σ_φ denote turbulence modeling constants. The turbulence model constants σ_φ and the source terms S_φ are given in Table 1,

Table 1: σ_φ and S_φ of incompressible transport equations

φ	σ_φ	S_φ
1	1.00	0
u	1.00	$-p_x + \nabla[\mu(u_j)_x]$
v	1.00	$-p_y + \nabla[\mu(u_j)_y]$
w	1.00	$-p_z + \nabla[\mu(u_j)_z]$
T	0.95	Φ
k	0.89	$\rho(P_k - \varepsilon)$
ε	1.15	$\rho(\varepsilon/k)(C_1P_k - C_2\varepsilon + C_3P_k^2/\varepsilon)$

where Φ is the energy dissipation function, P_k represents the turbulent kinetic energy production term, and C_1, C_2 and C_3 are model constants for the two-equation turbulence model. The present

computation solves the governing equations in dimensionless form. With constant-property assumption, energy equation is decoupled from other equations, so temperature field is solved subsequent to the attainment of a converged flowfield.

To solve the system of coupled nonlinear partial differential equations, it uses finite difference approximations to establish a system of linearized algebraic equations. An adaptive upwind scheme is utilized to model the convective terms of the momentum, energy and continuity equations, which is based on second and fourth order central differencing with artificial dissipation. Discretization of viscous fluxes and source terms uses a second-order central difference approximation. For velocity-pressure coupling, the present solution procedure employs a pressure-based, predictor followed by multi-corrector approach. Details of the present numerical methodology is given by Wang and Chen (1990) and Wang (1992).

Due to symmetry, the computational domain occupies the top half of the flow channel. Along all the solid walls, no-slip condition is applied for velocities, and temperature is assumed constant. For near-wall turbulence treatment, it uses a wall function with modified flux source and a velocity profile capable of providing a smooth transition between logarithmic law-of-wall and linear variation in viscous sublayer. Such a treatment significantly reduces the flux dependence on the near-wall spacing (Chen and Kim, 1987). The inlet conditions are fully developed profiles for velocities and turbulent parameters. These are resulted from a separate calculation for flow in a straight channel prior to the actual computations. Computations for all three turn configurations use the same number of grids, 65x41x21, distributed in the flow region, which is generated algebraically with significant packing in the turning regions. The Reynolds number based on the mean velocity and the channel width is 7.5×10^4, and the Prandtl number is 0.7 for air flow. All calculations were performed in a Cray XMP supercomputer. A converged solution for all variables requires approximately one hour of CPU time.

Using the straight-corner turn as a test case, three different grids; i.e., 51x11x11, 65x31x15, and 65x41x21 are chosen to examine the grid indepence. Results from such a comparative study indicate that differences among these grids have little impact on both momentum characteristics and heat transfer. The maximum changes in the perimeter-averaged, streamwise-resolved local heat transfer are about 11% between the coarsest grid and the intermediate grid, and 5% between the intermediate grid and the finest grid. The corresponding overall average changes are approximately 6% and 2% , respectively. The local maximum variations always occur in the downstream portion of the turn where the flow has probably the

most complex features over the entire computational domain. However, difference in the streamwise distribution of pressure coefficient is virtually unnoticeable.

RESULTS AND DISCUSSION

Figure 2 shows the velocity vectors in the turning region viewed on the central plane (x-y plane) of the duct. Upstream to the turning, all three cases exhibit similar flow behavior. Due to favorable longitudinal pressure gradient, flow near the inner wall experiences a slight acceleration. Conversely, because of the adverse pressure gradient, the flow near the outer wall decelerates. Inside and after the turn, the flow displays significantly different patterns between the cases of straight-corner and circular-corner. The rounded-corner turn, as expected, demonstrates flow features of those of the other two turn types combined. For both straight-corner and rounded-corner turns, recirculating zones exist near the upstream outer corner and adjacent to the tip of partition-wall. For the straight-corner turn, a rather weak recirculation appears in the downstream outer corner. Apparently, these geometry-induced flow separations are non-existent for the circular turn that has the smoothest turning profile. In the post-turn region, the circular-turn, on this particular viewing plane, has the strongest recirculation zone immediately adjacent to the partition wall. In fact, the other two cases also have very (even more) significant recirculation in the region, which is evident when viewed from other planes. Such an inclined recirculation is largely attributable to the fact that the mainstream is diverted by the sharp edge of the partition-wall, in conjunction with stronger turn-induced secondary flows as compared to the circular-corner turn.

One of the most intriguing features for flows through a bend is the existence of secondary flow, which moves along a direction perpendicular to that of the mainstream. Figures 3 to 5 show the evolution of the secondary flow pattern for all three turning shapes. The viewing orientation for these velocity-vector plots is chosen as one moves along the streamwise direction and is always facing downstream. Hence, for any viewing plane, the right sidewall is always the inner-wall and the left sidewall, on the other hand, is always the outer-wall. The four plots shown for each case represent different streamwise locations; i.e., (a) pre-turn, $x/D = 6$, (b) mid-turn, $y/D = 0$, (c) post-turn, $x/D = 6$, and (d) passage exit, $x/D = 0$. At the pre-turn location, secondary flow pattern is relatively insensitive to the difference in turn configuration. Here the mainstream begins to sense the turning, and the higher pressure near the outer wall forces the flow moving toward the inner wall. Boundary layer separation near the outer wall is evident for both straight-corner and rounded-corner turns; while, on the contrary, the circular-corner case shows no sign of such a separation.

As flow reaches the mid-plane of turning, a typical Dean-type recirculating pattern is clearly observed. This is known to be induced by the imbalance of centrifugal force and pressure gradient. The fluid in the channel core region experiences a larger centrifugal force than that near the wall. It is the differential of the centrifugal force and the pressure gradient that pushes the flow moving from the inner-wall toward the outer-wall. For a given z-coordinate, the pressure is greatest at the outer wall and smallest at the inner wall. Along the z-axis, the pressure is highest at the central plane (z/D = 0) and decreases toward the top wall. Hence a clockwise circulation is resulted as seen in the sub-figure (b) for all three turn configurations. However, with regard to the intensity of circulation, the circular-corner turn is the weakest, while the other two stronger cases are comparable. As a result of weak circulation, the center of circulation is closest to the top wall for the circular-corner turn. Another notable feature observed is the flow separation near the tip of the partition wall, which is most evident for the straight-corner turn, and virtually no separation exists in the circular-corner turn.

The post-turn secondary flow patterns become more complex, as the Dean-type circulation and the recirculating zone adjacent to the partition wall both appear in the region. Because the sense of rotation between these two flow features is opposite, a stagnant region is thus formed near the channel core (z/D = 0, about 1/3 from the inner wall), from which the flow splits and moves in opposite directions toward the sidewalls. The recirculating feature immediately adjacent to the partition wall is very dominating for both straight-corner turn and rounded-corner turn, while such a phenomenon is virtually absent for the circular turn. This represents a major effect of turn configuration on the flow structure in the post-turn region. According to Figure 2, the recirculating flow behind the partition wall for the circular turn is largely dominated by a vortex having its rotating axis normal to the x-y plane. As a sharp contrast, the rotating axis for the other two cases lies on the x-axis, along the mainstream direction. This further implies that much higher level of swirl exists in the post-turn recirculating region for both the straight-corner turn and rounded corner turn. At the channel exit, sub-figures (d), the secondary flow remains to bear the influence of Dean-type circulation. However, the differences in turn geometry virtually have no effect here.

It is understandable that the details in secondary flow pattern are largely dependent on the pressure distributions in the channel. Figure 6 reveals the local pressure coefficients on the two side walls along the channel central plane (z/D = 0). Note that the value of abscissa, ranging from 0 to 1.0 for all cases, is a dimensionless streamwise coordinate normalized by the total span of each sidewall. As expected, notable pressure differences between the two sidewalls exist in the

turning region, and they diminish as the overall pressure recovers toward the downstream of the second pass. The case with straight-corner turn has the greatest pressure drop over the entire channel; while the circular turn has the least drop. A somewhat surprising finding is that the rounded-corner turn reveals an overall pressure drop similar to that with the circular turn. For both straight-corner and rounded-corner configurations, pressure on the outer wall exhibits two local maxima in the turning region. The upstream minimum locates approximately in the mid-section of the turn, and the downstream one locates slightly downstream of the second corner. This is primarily caused by direct impingement of the mainstream as the flow is unable to negotiate the sharp turn. For all three cases studied, very low pressure coefficients consistently exist near the mid-section of the inner wall. However, according to the flow pattern shown in Figure 2, cause for such high pressure drops may vary with different turn geometries. For straight-corner and rounded-corner turns, it is attributable to the flow separation near the tip of the partition wall. For the circular-turn, the tip-induced separation is rather insignificant, so the pressure drop is primarily caused by flow acceleration near the tip.

The local heat transfer coefficient, h, is defined as

$$h = q / (T_w - T_i) \qquad (5)$$

where T_w and T_i represent the wall temperature and the flow inlet temperature, respectively. The values of both temperatures are kept as constant in the present study. The dimensionless heat transfer coefficient, Nusselt number, is defined as

$$Nu = hD/k \qquad (6)$$

Note that the present definition of h is different from the conventional way for internal flow, which typically uses the flow bulk temperature as the reference temperature. However, due mainly to complexity in flow direction, the bulk temperature near the turn is somewhat difficult to evaluate. The value of h or Nu under the present definition is linearly proportional to the magnitude of local heat flux.

Figure 7 displays the contours of Nu on the top wall over the entire channel. Although similar plots for the sidewalls are not given here, heat transfer characteristics on these surfaces generally follow the trends of top-wall Nu variation along the mainstream direction. For all the cases studied, heat transfer in the straight portion of the first pass reveals the thermally developing characteristics, as Nu decreases with the streamwise coordinate. Just prior to the

turning region, largely due to flow deceleration and separation, the magnitude of heat transfer coefficient on the channel outer wall decreases. On the contrary, the boundary layer flow acceleration enhances the heat transfer near the inner wall. Proceeding into the turn, heat transfer generally increases, but with severe local non-uniformity. Such a spatial non-uniformity is the strongest for the straight-corner turn, and the weakest for the circular turn. For the straight-corner case, the Nusselt number contours display two local maxima in the mid-turn and slightly downstream to the turn. Both locations coincide with the streamwise locations of the peak pressure on the outer wall. The two maxima appear to merge and shift slightly downstream for the rounded-corner turn. Such a single maximum zone locates further downstream for the circular turn. Despite different locations, the values of maximum heat transfer for all three cases are quite comparable, about twice as much the magnitude with fully-developed, straight channel flow. Another strong spatial-variation in Nusselt number lies in the region immediately behind the partition wall, where the recirculating flow results in low heat transfer in the region, less than half of its fully-developed counterpart in a straight duct. The size of such a low heat transfer zone is largest for the straight-corner turn, and the smallest for the circular turn. Accordingly, sharp tips for a partition wall may be undesirable as the internal passage cooling effectiveness is of concern.

Figure 8 shows the streamwise-resolved, perimeter-averaged Nusselt number, Nu_A, which is done by integrating the local Nusselt number on all participating walls at a given streamwise location. Note that here the reference temperature uses the bulk temperature for the definition of such a mean heat transfer coefficient. The resulting averaged Nusselt number is normalized by its fully developed counterpart in a straight duct without turn; i.e.,

$$Nu_o = 0.023\ Re^{0.8}\ Pr^{0.4} \qquad (7)$$

Also given in the figure is the regional average data from a recent experimental study by Chyu (1991). Note that the results from both experimental and numerical approaches agree very favorably. In the turning region, say $0.4 \le x/L \le 0.6$, the straight-corner turn has the highest heat transfer, while the circular turn has the lowest heat transfer, the difference between them is approximately 30%. The rounded-corner case falls slightly lower, by 5%, than the straight-corner case. However, in the post-turn region, heat transfer with circular turn surpasses that of the other two configurations, by almost the same amount of difference in the turning region. This implies that, from the standpoint of heat transfer enhancement, sharp corner turns may be more favorable for a short passage, and, on the other hand, a smooth corner turn is more beneficial for a long passage. Because of the aforementioned offset, heat transfer over the entire channel are

comparable within 8% for all the three cases studied. The straight-corner turn remains to be the highest (37% enhancement relative to the fully developed, straight channel flow), followed by the rounded-corner turn (31%), and the circular-corner turn (29%). If the issue of heat transfer per pumping power is of concern, a turn with rounded corners appear to be the best choice.

CONCLUDING REMARKS

Secondary flow and heat transfer in a two-pass, square duct with a 180-degree sharp turn are studied using a three-dimensional, numerical simulation. Particular emphasis is placed on the effects of three different turn configurations; i.e., (a) straight-corner turn, (b) rounded-corner turn, and (c) circular turn on the convective transport features in the duct. The computation employs a non-staggered grid, pressure-based, finite-difference method with an extended k-ε turbulence model to solve governing equations transformed in curvilinear coordinates. The computational results reveal detailed flow patterns and pressure characteristics near the turn. The secondary flow in the post-turn region shows combined features of a bend-induced, Dean-type circulation and a form-induced separation behind the partition wall. This effect varies significantly with different turn geometries. A turn with sharp corners; i.e. either straight or rounded corners, induces strong flow swirl in the second pass after the turn. Overall heat transfer stands greatly increased in the turning region; nevertheless, spatial variation in the local heat transfer is also very significant. The extent of local heat transfer variation depends strongly on the turn geometry and edge shape of the partition wall. The amount of heat transfer in the turning region is generally higher for the straight-corner and rounded-corner turns than for the circular turn, by approximately 30% in the present case. However, in the post-turn region and the second-pass, heat transfer with circular turn surpasses that of the other turn configurations, by almost the same difference in the turning region. Hence, heat transfer over the entire channel are comparable within 8% for all the three cases studied. Regional-average heat transfer results from the present computation agree favorably with those from the experimental measurements.

REFERENCES

Baughn, J.W., Iacovides, H., Jackson, D.C. and Launder, B.E., 1987, "Local Heat Transfer Measurements in Turbulent Flow Around a 180-deg Pipe Bend," J. Heat Transfer, Vol. 109, pp.43-48

Boyle, R.J., 1984, "Heat Transfer in Serpentine Passages with Turbulence Promoters," ASME 84-HT-24

Chen, Y.S. and Kim, S.W., 1987, "Computation of Turbulent Flows Using an Extended k-e Turbulence Model," NASA CR-179204.

Chen, Y.S., 1989, "Compressible and Incompressible Flow Computations with a Pressure Based Method," AIAA-89-0286

Cheng, K.C., and Akiyama, M., "Laminar Forced Convection Heat Transfer in Curved Rectangular Channels," *Int. J. Heat Mass Transfer,* Vol. 13, 1970, pp. 1787-1806.

Cheng, K.C., Shi, L., Kurokawa, M., and Chyu, M.K., 1992, "Visualization of Flow Patterns in a 180-Degree Sharp Turn of a Square Duct," Fourth International Symposium on Transport Phenomena and Dynamics of Rotating Machinery, Honolulu, April 5-8, 1992.

Chyu, M.K., 1991, "Regional Heat Transfer and Pressure Drop in Two-Pass and Three-Pass Flow Passages with 180-Degree Sharp Turns," *J. Heat Transfer*, 113, pp. 63-70.

Dean, W.R. and Hurst, J.M., "Note on the Motion of Fluid in a Curved Pipe, " *Mathematika*, Vol. 6, 1959, pp. 77-85.

Fan, C.S. and Metzger, D.E., 1987, "Effects of Channel Aspect Ratio on Heat Transfer in Rectangular Passage Sharp 180-Deg Turns", ASME Paper 87-GT-113.

Humphrey, J.A.C., Taylor, A.M.K. and Whitelaw, J.H., 1977, "Laminar Flow in a Square Duct of Strong Curvature," *J. Fluid Mech.*, Vol. 83, pp. 509-527.

Jiang, Y., Chen, C.P. and Chyu, M.K., 1990, "A Numerical Computation of Convective Heat Transfer in Two-Pass Rectangular Channels with a 180-Degree Sharp Turn," AIAA-90-0355

Johnson, R.W. and Launder, B.E., 1985, "Local Nusselt Number and Temperature Field in Turbulent Flow through a Heated Square-Sectioned U-Bend," *Int. J. Heat & Fluid Flow*, Vol. 6, pp. 171-180.

Johnson, R.W., 1988, "Numerical Simulation of Local Nusselt Number for Turbulent Flow in a Square Duct with a 180° Bend," *Numerical Heat Transfer,* Vol. 13, pp. 205-228.

Metzger, D.E., Pelvich, C.W., and Fan, C.S., 1984, "Pressure Loss Through Sharp 180 Degree Turns in Smooth Rectangular Channels," *J. Engr. for Gas Turbines and Power,* Vol. 106, 1984, pp. 677-681.

Metzger, D.E. and Sahm, M.K., 1986, "Heat Transfer Around Sharp 180-Deg Turns in Smooth Rectangular Channels", *J. Heat Transfer, Transfer*. Vol. 108, pp. 500-506.

Mori, Y. and Nakayama, W., 1967, "Study on Forced Convective Transfer in Curved Pipes (2nd Report, Turbulent Region)," *Int. J. Heat and Mass Transfer,* Vol.10, pp. 37-59.

Mori, Y and Nakayama, W., 1971, "Study on Forced Convective Transfer in a Curved Channel With A Square Cross Section," *Int. J. Heat and Mass Transfer,* Vol. 14, pp. 1787-1805

Murthy, J.Y. and Chyu, M.K., 1987, "A Numerical Study of Laminar Flow and Heat Transfer in a Channel with a 180-Deg Bend," ASME Paper 87-HT-7

Wang, T.S. and Y.S. Chen, 1990, "A Unified Navier-Stokes Flowfield and Performance Analysis of Liquid Rocket Engines," AIAA-90-2494

Wang, T.S., 1992, "Numerical Study of The Transient Nozzle Flow Separation of Liquid Rocket Engines," Computational Fluid Dynamics J., Vol. 1, No. 3, pp. 305-314.

FIGURES

Fig. 1 Turn Configuration

a) Straight-corner Turn
b) Rounded-corner Turn
c) Circular-corner Turn

Fig. 2 Velocity Vector on Center Plane (z/D = 0)

a) Straight-corner Turn
b) Rounded-corner Turn
c) Circular-corner Turn

Fig. 3 Secondary Flow with Straight-corner Turn

Fig. 4 Secondary Flow with Rounded-corner Turn

Fig. 5 Secondary Flow with Circular-corner Turn

Fig. 6 Pressure Coefficient

Fig. 7 Local Nusselt Number Distribution

a) Straight-corner Turn
b) Rounded-corner Turn
c) Circular-corner Turn

Fig. 8 Streamwise-Resolved Average Nusselt Number

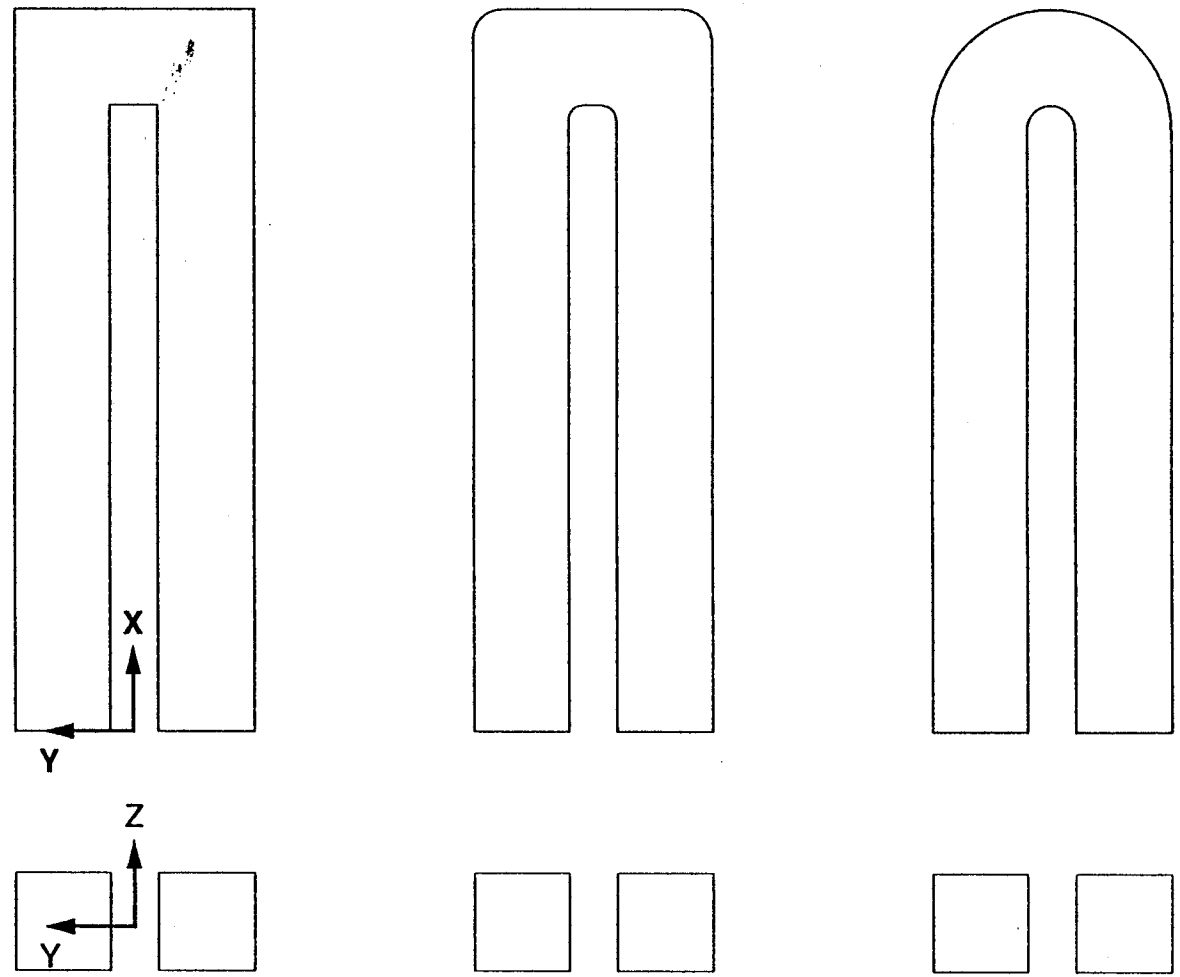

FIGURE 1 Turn Configurations

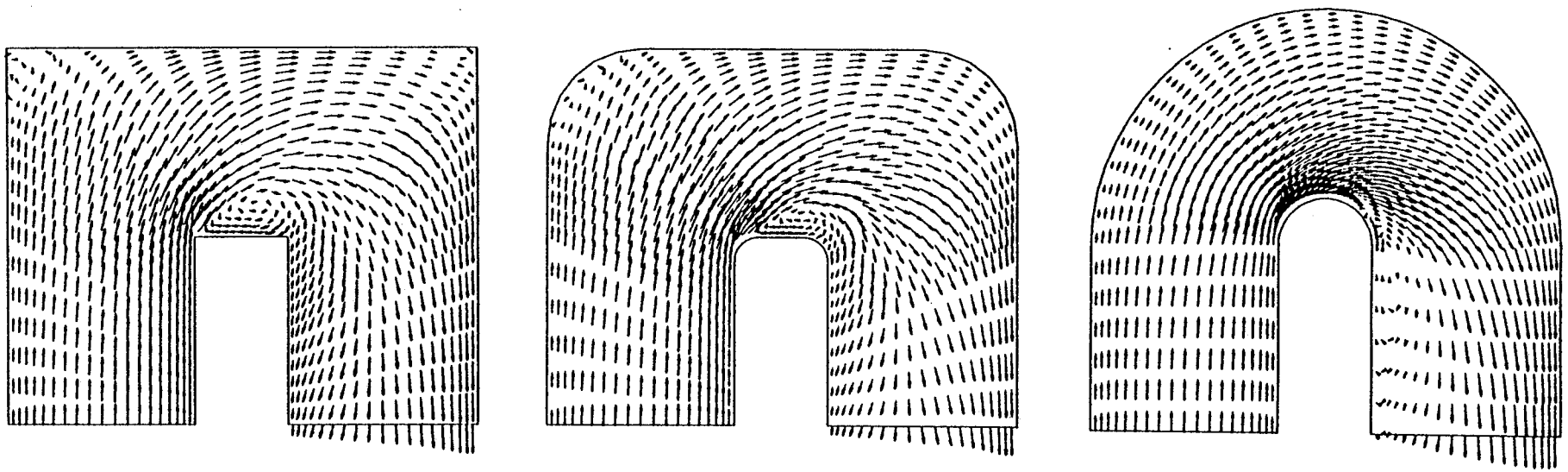

FIGURE 2 Velocity Vector on Center Plane (z=0)

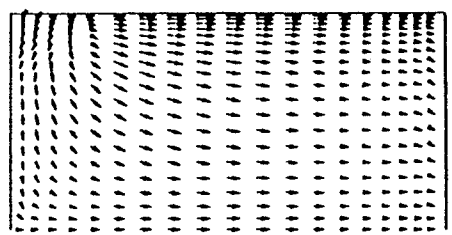

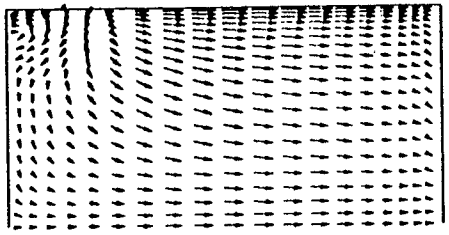

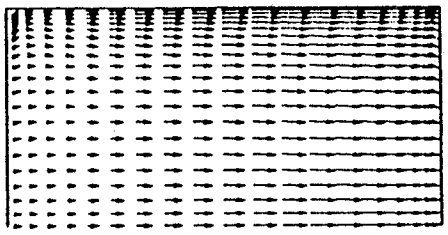

(a)
Pre-
Turn

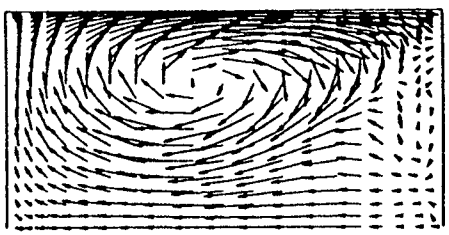

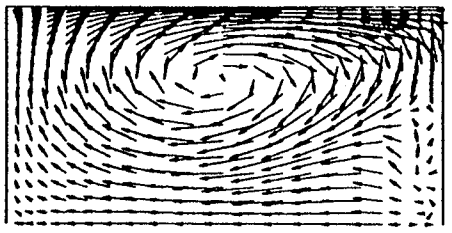

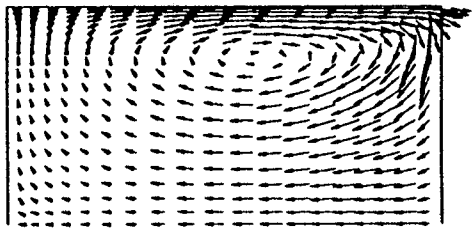

(b)
Mid-
Turn

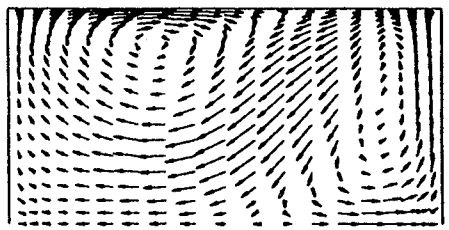

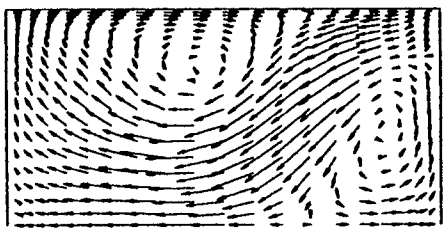

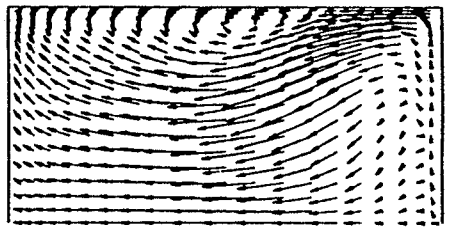

(c)
Post-
Turn

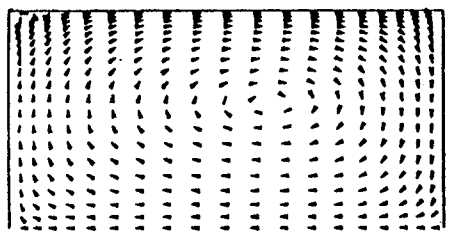

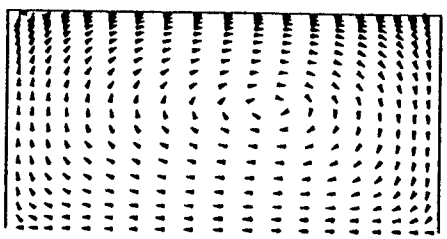

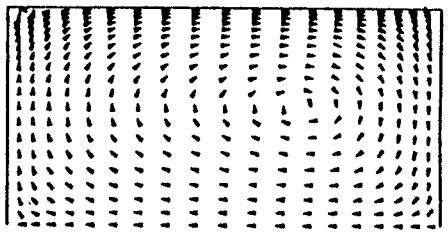

(d)
Passage
Exit

Straight-Corner

FIGURE 3

Rounded-Corner

FIGURE 4

Circular-Corner

FIGURE 5

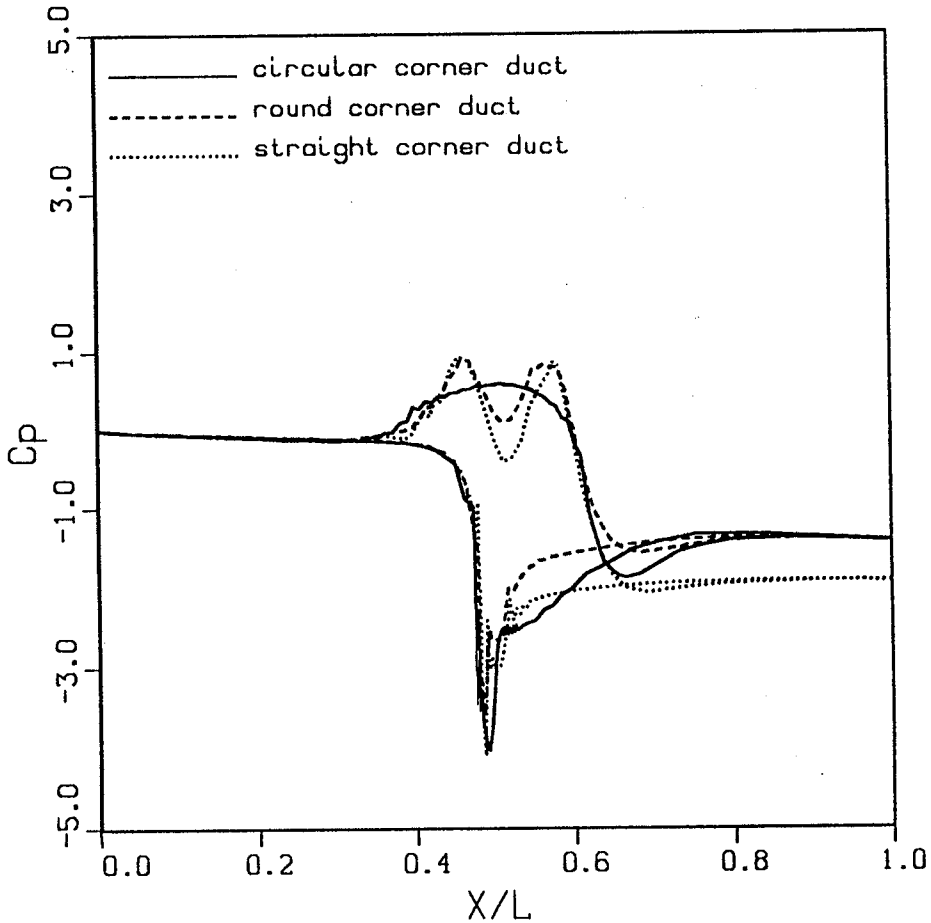

FIGURE 6 Pressure Coefficient

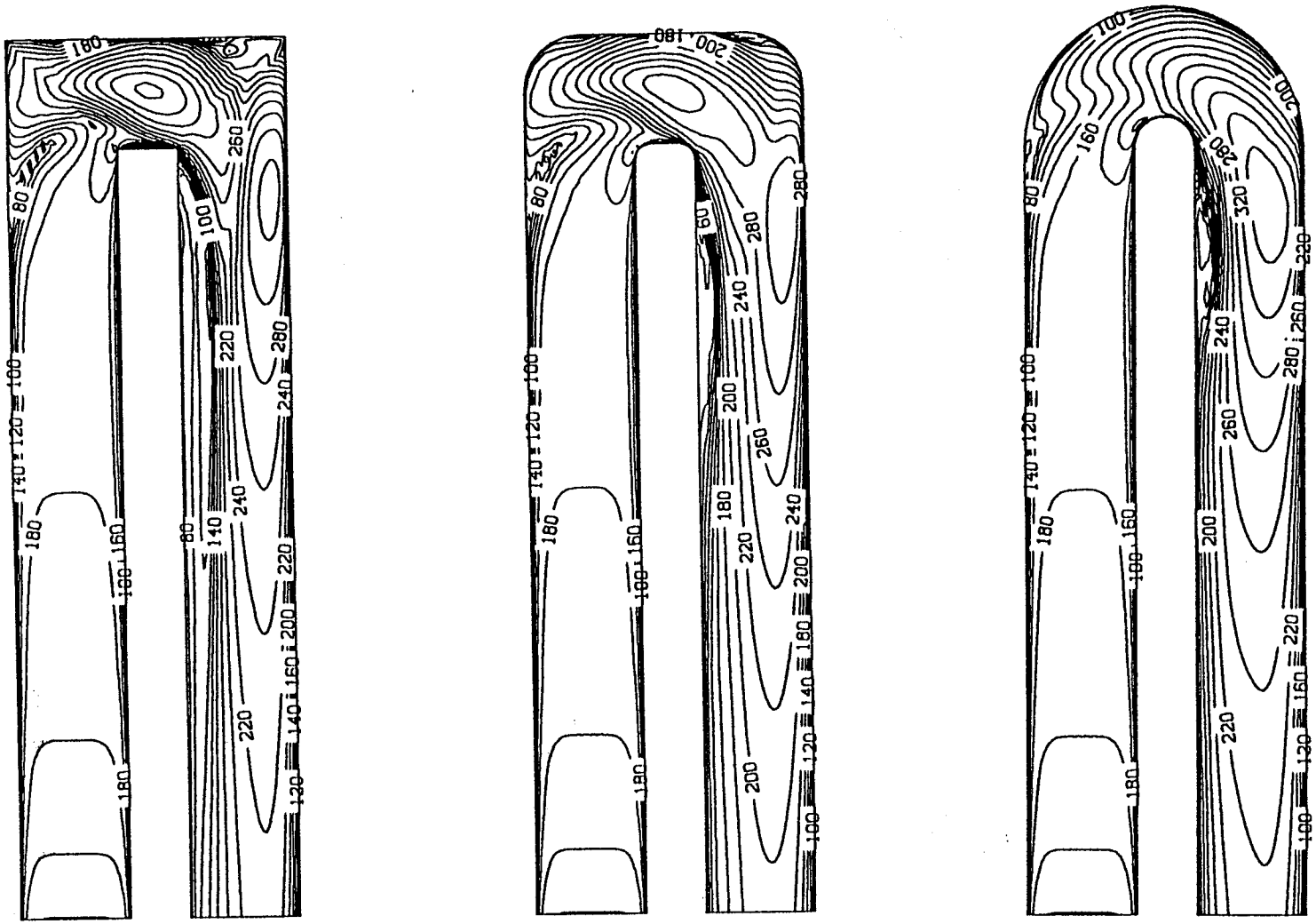

FIGURE 7 Local Nusselt Number Distribution

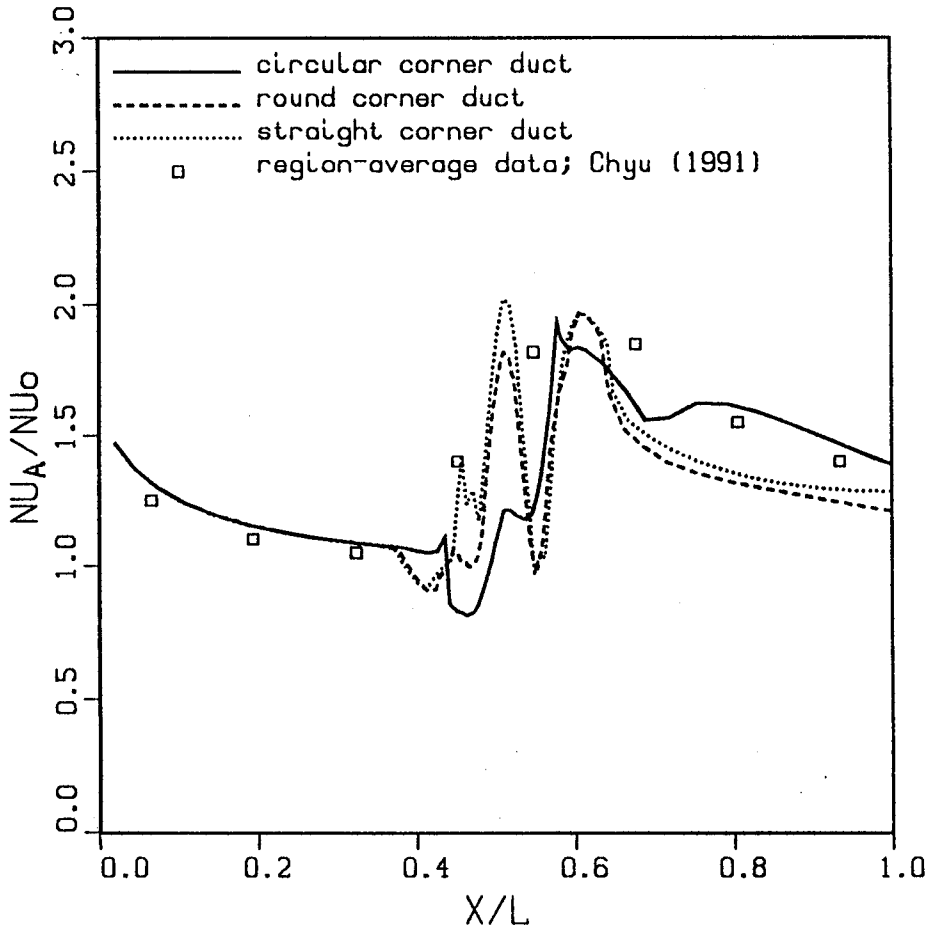

FIGURE 8 Streamwise-Resolved Average Nu